NASA TECHNICAL MEMORANDUM

NASA TM X-73,166

NASA TM X-73,166

SULFIDATION OF 310 STAINLESS STEEL AT SULFUR POTENTIALS ENCOUNTERED IN COAL CONVERSION SYSTEMS

D. Bhogeswara Rao
Ames Research Center, Moffett Field, California 94035 and
Department of Materials Science and Engineering
University of California, Berkeley, California 94720

and

Howard G. Nelson
Ames Research Center
Moffett Field, California 94035

September 1976

1. Report No.	2. Government Accession No.	3. Recipient's Catalog No.
NASA TM X-73,166		

4. Title and Subtitle	5. Report Date
SULFIDATION OF 310 STAINLESS STEEL AT SULFUR POTENTIALS ENCOUNTERED IN COAL CORROSION SYSTEMS	6. Performing Organization Code

7. Author(s)	8. Performing Organization Report No.
D. Bhogeswara Rao* and Howard G. Nelson**	A-6723
	10. Work Unit No. 778-11-02

9. Performing Organization Name and Address	11. Contract or Grant No.
*Ames Research Center, NASA, Moffett Field, California 94035 and Department of Materials Science and Engineering University of California, Berkeley, California 94720 **Ames Research Center, NASA, Moffett Field, California 94035	13. Type of Report and Period Covered Technical Memorandum

12. Sponsoring Agency Name and Address	14. Sponsoring Agency Code
National Space and Aeronautics Administration Washington, D.C. 20546	

15. Supplementary Notes

16. Abstract

The sulfidation of SAE 310 stainless steel was carried out in gas mixtures of hydrogen and hydrogen sulfide over a range of sulfur potentials anticipated in advanced coal gasification processes. The kinetics, composition, and morphology of sulfide scale formation were studied at a fixed temperature of 1065 K over a range of sulfur potentials from 1.5×10^{-4} Nm^{-2} to 9×10^{2} Nm^{-2}. At all sulfur potentials investigated, the sulfide scales were found to be multilayered. The relative thickness of the individual layers as well as the composition was found to depend on the sulfur potential. The reaction was found to obey the parabolic rate law after an initial transient period. Considerably longer transient periods were found to be due to unsteady state conditions resulting from compositional variations in the spinel layer. The sulfur pressure dependence on the parabolic rate constant was found to best fit the equation

$$K_p = \text{Const.}\, P_{S_2}^{1/n}$$

where n equals 3.7. The growth of the outer layers was found to be primarily due to the diffusion of metal ions, iron being the predominant species. The inner layer growth was due to the dissociation of the primary product at the alloy-scale interface and depended on the activity of chromium.

17. Key Words (Suggested by Author(s))	18. Distribution Statement
Corrosion of 310 stainless steel Kinetics of sulfidation Nature of sulfide scales Morphology of sulfide scales Mechanism of sulfidation	Unlimited STAR Category – 26

19. Security Classif. (of this report)	20. Security Classif. (of this page)	21. No. of Pages	22. Price*
Unclassified	Unclassified	30	$3.75

*For sale by the National Technical Information Service, Springfield, Virginia 22161

SULFIDATION OF 310 STAINLESS STEEL AT SULFUR POTENTIALS ENCOUNTERED IN COAL CONVERSION SYSTEMS

D. Bhogeswara Rao and Howard G. Nelson

Ames Research Center, NASA, Moffett Field, California 94035 and
Department of Materials Science and Engineering
University of California, Berkeley, California 94720

Ames Research Center, NASA, Moffett Field, California 94035

ABSTRACT

The sulfidation of SAE 310 stainless steel was carried out in gas mixtures of hydrogen and hydrogen sulfide over a range of sulfur potentials anticipated in advanced coal gasification processes. The kinetics, composition, and morphology of sulfide scale formation were studied at a fixed temperature of 1065 K over a range of sulfur potentials from 1.5×10^{-4} Nm^{-2} to 9×10^{2} Nm^{-2}. At all sulfur potentials investigated, the sulfide scales were found to be multilayered. The relative thickness of the individual layers as well as the composition was found to depend on the sulfur potential. The reaction was found to obey the parabolic rate law after an initial transient period. Considerably longer transient periods were found to be due to unsteady state conditions resulting from compositional variations in the spinel layer. The sulfur pressure dependence on the parabolic rate constant was found to best fit the equation

$$K_p = \text{Const.}\ P_{S_2}^{1/n}$$

where n equals 3.7. The growth of the outer layers was found to be primarily due to the diffusion of metal ions, iron being the predominant species. The inner layer growth was due to the dissociation of the primary product at the alloy-scale interface and depended on the activity of chromium.

INTRODUCTION

Corrosion problems encountered in coal conversion systems can be severe and complex, primarily because of the extremes of temperature, pressure, and gas compositions. McNab[1] has given the gas compositions of the five major coal conversion processes, all containing molecular species based on oxygen, hydrogen, carbon, nitrogen, and sulfur. These chemical species could act individually or collectively to degrade the structural integrity of the coal conversion system. Of the chemical species present, sulfur is probably

the most unwanted. Degradation of a metal by the formation of a sulfide scale is more severe than that due to the formation of an oxide for the following reasons:

1. Because of the excessively high volume quotient of sulfide scales compared with oxides, stresses are developed that lead to cracks and fractures of the sulfide layer, making it porous and nonprotective.

2. The sulfides in general have lower melting points than oxides, thus reducing the strength of the scales and limiting their usefulness at high temperatures. The melting points of many sulfides are further reduced by the formation of eutectics with the neighboring metal.

3. The rates of sulfide formation are generally much more rapid than those of oxides.

4. Reliable thermodynamic and solubility data are not available in the literature, making it impossible to predict the composition of the sulfide scales. Additionally, not all sulfide compounds have been identified, making characterization difficult and cumbersome.

Most previous sulfidation studies have been conducted on either pure metals or binary alloys[2,3] with little attention paid to the more complex alloys such as those being used in coal conversion pilot-plant operation. An understanding of the sulfidation kinetics and of the morphology and nature of sulfide scale formation in these complex alloys is essential to an evaluation of the severity of corrosion that will occur in coal conversion systems. As part of a continuing program on the subject, the sulfidation of SAE 310 stainless steel in gas mixtures of hydrogen sulfide and hydrogen is being investigated. The present study deals with the specific influence on sulfur potential (partial pressure) on the kinetics of scale formation and on the nature and morphology of scale layers.

MATERIALS AND APPARATUS

Commercially produced, cold-rolled, SAE 310 stainless steel was used in this study and had the composition shown in Table 1. Test coupons 2 cm by 1.25 cm by 0.33 cm were polished through 1-μ diamond abrasive and degreased thoroughly by washing in acetone. Coupon dimensions were measured to an accuracy of 0.001 cm by use of a micrometer, and the surface area was calculated.

Commercially available high-purity hydrogen and hydrogen sulfide gases were used and were further purified by passing them through a purification train designed to remove residual water vapor and oxygen. Gas flow rates were monitored and controlled by an electronic control system.

Sulfidation kinetics were measured using the weight gain technique. Weight change was continuously monitored to a sensitivity of 0.1 mg. The balance system was purged with argon to avoid condensation of sulfur and any reaction with the balance components. At the same time, sufficient precautions were taken not to dilute the test gas mixture.

A recrystallized alumina tube, 5 cm in diameter, served as a reaction chamber. The chamber was connected to the balance unit by means of a gastight, 'O'-ring seal. The reaction chamber was surrounded by a resistance furnace. Furnace temperature control was achieved by the potentiometric controller in conjunction with a chromel-alumel thermocouple positioned close to the furnace windings. Temperature was found to be uniform within ±1°C over the middle 5 cm of the reaction chamber. The actual coupon temperature was estimated by means of two Pt-Pt10%Rh thermocouples located near both ends of the coupon. It is estimated that coupon temperature was kept constant to within ±3°C during any run.

EXPERIMENTAL PROCEDURE

The test coupon, suspended from one arm of the balance by an alumina-sheathed platinum wire, was lowered into the constant temperature zone of the reaction chamber. At the higher sulfur pressures where some reaction with platinum was noticed, a gold wire was used. The coupon was brought to the desired temperature under a vacuum of better than 10^{-4} Nm^{-2}. Argon was then passed through the balance assembly, and at the same time hydrogen was passed through the reaction chamber to reduce any oxide traces that may have formed during handling of the coupon. The reaction gases at the desired ratio of hydrogen to hydrogen sulfide were allowed to mix in a mixing chamber. The experiment was initiated at the moment the reactive gas mixture was allowed to pass through the reaction chamber. During all experiments, a constant reactive gas flow rate of 500 cc min^{-1} or greater was maintained. At the end of each run the flow of reactive gas was halted and argon flow was resumed while the coupon was being cooled. When the system had attained room temperature, the coupon was removed and the corrosion product was examined. The continuously recorded weight gain data were used to calculate the appropriate rate equations.

Marker experiments were conducted using platinum wire markers spot welded to the coupon surface. At the end of an experiment the coupon was sectioned with a diamond saw, mounted, polished, and examined using metallographic techniques. In many cases, the scales flaked off during cooling: such scales were collected and examined separately from the unreacted alloy.

The morphology and the composition of the scales were examined using scanning electron microscopy and energy dispersive x-ray analysis. To permit quantitative analysis, FeS_2 was used as a sulfur standard and the SAE 310 stainless steel was used as a standard for iron, nickel, and chromium. At very high sulfur concentrations, x-ray dispersive analysis failed to yield accurate results. Consequently, electron microprobe analysis was used for quantitative determination of the compositions. In all cases atomic absorption and fluorescent effects were eliminated using appropriate computer programs.

The sulfide phases present in these scales were identified using x-ray diffraction techniques. In most of the cases it was possible to identify these phases by comparison with the ASTM powder diffraction file.

RESULTS

A wide range of sulfur potentials (partial pressures) is encountered in the various coal gasification processes. The partial pressures of sulfur were calculated from the listed gas compositions of the five major gasification processes using the equilibrium relationship

$$H_2S(g) \rightleftharpoons H_2(g) + 1/2\ S_2(g) \qquad (1)$$

where the dimeric sulfur species was assumed to be the predominant species. The free energy functions for these calculations were taken from the JANAF tables.[4] From the equilibrium constant at a given temperature, the sulfur potential was obtained by adjusting the ratio of the partial pressure of hydrogen to the partial pressure of hydrogen sulfide. It is evident from Fig. 1 that, at any given temperature, the sulfur partial pressure can vary over a range as large as 4 orders of magnitude or more depending on the particular process under consideration.

Reaction Kinetics

Sulfidation kinetics as a function of partial pressure of sulfur were studied over the pressure range from 1.5×10^{-4} Nm^{-2} to 9×10^{2} Nm^{-2} at 1065 K. At a constant sulfur partial pressure, weight gain per unit area was found to exhibit two distinct regions: an initial transient region, and steady-state or final region. The transition from one region to the other appears to occur at a weight gain of 30-40 mg cm^{-2} and shows some dependence on sulfur pressure. The reaction rate data were analyzed to determine the appropriate rate equations. The final region appears to obey parabolic rate kinetics as shown in Fig. 2, which is a plot of the square of weight gain per unit area vs time. Within the transient region another parabolic region could be found or, alternatively, the transient period could be represented by a logarithmic equation; for consistency the former was preferred. The two parabolic regions are referred to hereafter as parabolic I and parabolic II. From the straight portions of regions I and II (Fig. 2), the parabolic rate constants were calculated. The relationship between the parabolic rate constants and the sulfur partial pressure is shown in Fig. 3. From the straight line portions of the curve the data was found to be best represented by an equation of the form

$$K_p = \text{Const.}\ P_{S_2}^{1/n} \qquad (2)$$

where n equals 3.9 in region I and 3.7 in region II.

Scale Morphology

At all sulfur pressures investigated the sulfide scales were found to be multilayered and highly porous. Porosity was particularly associated with the interfaces between the different layers. In many cases the different layers were separated by large fissures and often became detached from the unreacted alloy as a result of either mechanical or thermal stresses. In all cases, scales became detached from the unreacted alloy at the coupon corners.

The relative amount of the various layers present in the scale was found to be dependent upon the partial pressure of sulfur. The microstructures of the scales formed at four different sulfur pressures at a constant temperature of 1065 K are shown in Fig. 4; it can be seen that at higher sulfur potentials ($P_{S_2} > 10^{-3}$ Nm^{-2}) three layers are present in the sulfide scale. Additionally, the relative thicknesses of the individual layers are seen to vary with sulfur pressure. The outer layer is seen to decrease in thickness as the sulfur potential is decreased, whereas the intermediate layer is increased and the inner layer remains essentially constant for a given degree of reaction. At the lower potentials investigated ($P_{S_2} < 10^{-3}$ Nm^{-2}), the outer layer in the sulfide scale disappeared completely. At very high sulfur partial pressures ($P_{S_2} > 10^{-1}$ Nm^{-2}), the outer layer of the sulfide scale became extremely thick and could be mechanically separated from the remaining layers. Whenever an outer layer was formed, it was bronze in color. When the outer layer did not form, the corrosion product appeared to be silver white. The interface between the middle layer and the inner layer was either grey or dark.

Sulfide Phases

The various layers of the sulfide scales were mechanically separated and examined by x-ray diffraction analysis in order to identify the different sulfide phases present. In all cases the innermost layer was adherent to the unreacted alloy and was removed by scraping. The x-ray diffraction patterns shown in Fig. 5 are of the layers of scale formed at 1065 K in a sulfur pressure of 1.8 Nm^{-2}. The diffraction pattern of the outer layer shown in Fig. 5a was identified as iron, nickel sulfide ($(Fe,Ni)_9S_8$, Pentlandite, ASTM 8-90) with cubic symmetry. The diffraction pattern of the middle layer is shown in Fig. 5b and was identified as that or iron, chromium sulfide spinel ($FeCr_2S_4$, Daubreelite, ASTM 4-0651). The actual composition of this phase as determined by electron microprobe analysis was found to differ from the spinel composition, $FeCr_2S_4$. Although this layer appears to contain a single phase, the composition of this phase was dependent on the partial pressure of sulfur. This phase has an extended solubility for iron sulfide and could better be represented by the formula $Fe(Fe_{2-x}Cr_xS_4)$. The diffraction pattern for a mixture of the outer and middle layers is shown in Fig. 5c.

The diffraction pattern for the inner layer is shown in Fig. 5d and is composed mainly of the spinel and chromium sulfides. The chromium sulfide phase was mainly present near the interface of the unreacted metal and the inner layer. Because the binary Cr-S system is complicated by the presence of a number of phases, each stable in a narrow range of composition,[5] it was impossible to ascertain the exact phases present in the inner layer by x-ray diffraction analysis. From a combination of energy dispersive x-ray analysis, microprobe analysis and x-ray diffraction analysis, it was determined that the composition of the chromium sulfide phase is either Cr_2S_3 or Cr_5S_6. Additionally, small amounts of iron, present in this inner layer, made analysis even more difficult. The nature of the inner layer was found to depend on the partial pressure of sulfur. Sulfur pressures of about 40 Nm^{-2} and above led to the formation of sublayers within the inner layer; the sublayers were continuous. At sulfur potentials lower than 1.8 Nm^{-2} the inner layer consisted of a randomly distributed spinel and of the chromium sulfide phases imbedded in a metal matrix which was rich in iron and nickel (Fig. 6). Additionally, the relative area occupied by the sulfide phase in the inner layer was found to depend on the sulfur pressure: the lower the

sulfur pressure the lesser the inclusions. The exact metal composition was also found to be dependent upon whether an outer layer existed and thus, upon the partial pressure of sulfur at which the scale is formed.

Variations in sulfur partial pressure were found to influence the phases present in the outer layer. Scales formed at a sulfur partial pressure of 9×10^{2} Nm^{-2} were found to exhibit an outer layer corresponding to iron sulfide ($Fe_{(1-x)}S$, Pyrrhotite, ASTM-17-201) having a constant shift in d-spacings and no lines corresponding to nickel sulfide. Energy dispersive x-ray analysis, however, showed the presence of nickel and it was concluded that this is a solid solution of nickel sulfide in iron sulfide.

Scale Microstructure

Because the various layers of the sulfide scales could be mechanically separated, the microstructures and compositions of these surfaces were studied in detail using scanning electron microscopy and energy dispersive x-ray analysis. For the reaction carried out at a sulfur potential of 9×10^{2} Nm^{-2} for 5 hr at a temperature of 1070 K, three distinct sulfide layers were formed. The top surface of the outer layer adjacent to the gas phase is shown in Fig. 7. The microstructure of this layer consists of large columnar grains extending from the surface (Fig. 7a). Energy dispersive x-ray analysis of the large columnar grain of Fig. 7a indicates that this layer consists primarily of the $Fe_{(1-x)}S$ phase which also contain some nickel (Fig. 7c). Grain boundaries are clearly evident, many of which contain large cracks (Figs. 7a, b, and d). As suggested by the number of such cracks, the outer layer was very friable and easily separated from the middle layer. The microstructure and composition of the bottom surface of the outer layer is shown in Fig. 8. At this location the outer layer appears to be fairly continuous and contains only a few holes. Energy dispersive x-ray analysis of the overall surface shown in Fig. 8a indicates a composition similar to the top surface of this layer except that chromium was also observed (Fig. 8c). After a detailed compositional analysis of the microstructure, it was determined that the presence of chromium was the result of a few isolated grains attached to the surface from the intermediate layer (Figs. 8b and d).

The microstructure of the top and bottom surface of the middle layer is shown in Fig. 9. The top surface of the middle layer was found to be porous and granular with well defined facets (Fig. 9a). EDAX analysis of the overall surface (Fig. 9b) showed the presence of all elements, that is, sulfur, chromium, iron, and nickel. More detailed analysis, however, suggests that this surface is made up of a number of grains having different compositions. As an example, the crystallite indicated by the arrow in Fig. 9a was found to contain far less sulfur and more iron (Fig. 9c) than the overall composition of this surface (Fig. 9b). The microstructure and composition of the bottom surface of the middle layer is shown in Figs. 9d and 9e. As can be seen, this surface is very fine grained compared to the outer surfaces and consists almost entirely of sulfur and chromium. Finally, the top surface of the sulfide layers adhering to the unreacted alloy was found to be identical to the bottom surface of the middle layer (Figs. 9d and 9e).

Sulfide scales formed at sulfur potentials from 1.8 Nm^{-2} to 10^{-3} Nm^{-2} exhibited an outer layer similar in microstructure and composition to that formed at the highest sulfur

potential (Fig. 7) except that extensive outgrowth of columnar crystals from the outer surface was not significant (Figs. 10a and 10b). The microstructure and composition of the intermediate layer was also found to be similar to that observed at the highest sulfur partial pressure except that this layer is more continuous (Figs. 10c and 10d). No differences were observed in the microstructure or composition of the inner layer surfaces at these sulfur potentials.

Sulfide scales formed at sulfur potentials lower than 10^{-3} Nm^{-2} exhibited only what was termed, at higher sulfur pressures, an intermediate layer and an inner layer. Figure 11 shows the microstructure and composition of the top surface (Fig. 11a, a′, and a″), and of the bottom surface (Figs. 11b, b′ and b″) of this intermediate layer. As shown in Fig. 11, the top surface of this intermediate layer is smooth, large grained, and contains some cracks at the grain boundaries. Some small outgrowths, seen on the top surface, appear to be secondary in origin. These outgrowths contained a considerable amount of manganese (Fig. 10a′). The inner layer is jagged and facetted.

Composition Profiles

Concentration profiles across the various layers of the sulfide scales were established using an electron microprobe analysis. At high sulfur partial pressures (greater than 10^{-3} Nm^{-2}) the outer layer, consisting of FeS and $(Fe,Ni)_9S_8$ phases, yields compositions of 41% S, 42% Fe, 14% Ni, 2.9% Cr for the FeS phase and of 37% S, 45% Fe, 14% Ni, and 3% Cr for the $(Fe,Ni)_9S_8$ phase. At lower sulfur potentials, where the outer layer is no longer present, concentration profiles for iron, chromium, nickel, and sulfur are shown in Fig. 12. This sample was exposed to sulfur at 1×10^{-3} Nm^{-2} for 10 hr at 1065 K. As seen in Fig. 12, the composition of the outer layer (equivalent to the intermediate layer at higher sulfur partial pressures) corresponds to that of a mixed spinel. The composition of this phase is seen to vary gradually; chromium increasing and iron decreasing as we move away from the outer surface (the gas-scale interface). Sulfur and nickel compositions are seen to remain essentially constant at 42% and 3%, respectively. This suggests a wide range of homogeneity for the spinel which is best represented by $Fe(Fe_{2-x}Cr_xS_4)$. The inner layer formed at this partial pressure (1×10^{-3} Nm^{-2}) is made up of sulfide inclusions in an alloy phase, and accounts for the wide variation in composition in this region shown in Fig. 12. The sulfide inclusions have the composition of 38% S, 42% Cr, and 20% Fe with negligible amounts of nickel present. The alloy surrounding this phase is seen to be rich in nickel and iron and to have the composition 46% Ni, 40% Fe, 8% Cr, and 6% S. (At higher sulfur potentials, where three sulfide layers exist, the alloy phase was found to be higher in iron concentration.) As seen in Fig. 12, between 100 and 140 μ from the unreacted alloy, the sulfide phase is primarily chromium sulfide having the composition Cr_5S_6. As the sulfur potential is further reduced to 1.5×10^{-4} Nm^{-2}, the outer layer (the intermediate layer at highest sulfur potential) has the composition 40% S, 23% Cr, 26% Fe, and 0.5% Ni with the inner layer unchanged.

Sulfide Layer Growth

In an effort to understand the sequence of layer formation, sulfide scales were studied as a function of time at a sulfur potential of 1.4×10^{-2} Nm^{-2}. At this sulfur potential three

sulfide layers were formed; they are shown in Fig. 13. During initial stages of scale formation (up to 80 min corresponding to the transient period), the middle and inner layers are formed and grow with time, the middle layer growing more rapidly. At the end of this period, inner layer growth ceases and, simultaneously, outer layer growth begins.

Platinum markers were used in an effort to identify the direction of the layer growth. During the course of the sulfidation reaction at all sulfur potentials, the markers became buried at the interface of the intermediate and inner layers (between the mixed spinel and the chromium sulfide phases) as is shown in Fig. 14. As can be seen in this figure, fissures were formed at the interface and were located either above the markers or below the markers. In the former case scale growth was affected and in the latter case no detectable influence was noticed.

DISCUSSION

The sulfidation of SAE 310 stainless steel at various sulfur potentials has been found to be extremely complex, and, unfortunately, there is no companion study in the literature for comparison. From the chemical composition of this alloy (Table 1) it is evident that there exist eight metallic elements that could influence the growth of sulfide scales. In general, however, elements in concentration less than 2% will influence only the rate of scale growth and should not participate in the formation of a sulfide phase. This leaves the three major components of the alloy (Ni, Cr, and Fe) as the potential sulfide phase formers. Our present knowledge of sulfidation is limited to the binary alloy systems of Fe-Cr and Ni-Cr.

Comparison with Binary Alloy Systems

Mrowec et al.[6] and Narita and Nishida[7] have studied the sulfidation of Fe-Cr alloys under 1 atm of pure sulfur vapor. Zelouf and Simkovich[8] also studied the sulfidation of Fe-Cr alloys in H_2-H_2S gas mixtures. Similar to the present observations on SAE 310 stainless steel, all investigators observed that the rate of sulfidation could be expressed by a parabolic relationship after an initial transient period. The reaction rate observed in the present work is comparable to that reported by Zelouf and Simkovich[8]; however, no information was reported by these authors on the nature of the scales. Mrowec et al.[6] reported that the sulfide scales contained two layers: an outer FeS layer and an inner mixed spinel layer having the composition $Fe(Fe_{2-x}Cr_xS_4)$. Narita and Nishida[7] observed a three-layer scale for the Fe-Cr alloy having a chromium content similar to that of SAE 310 stainless steel. In this case, the outer sulfide layer consisted of a pure FeS phase, and the inner and intermediate layers contained FeS, $FeCr_2S_4$, and Cr_3S_4. Strafford and Manifold,[9] in studies on the Fe-Cr system containing 5% chromium, found the existence of mixed sulfides (FeS and Cr_2S_3) in the inner layer instead of the spinel phase. In the present investigation at the highest sulfur potential (9×10^2 Nm^{-2}) the outer layer of the three layer structure was found to consist of iron sulfide, FeS, similar to that observed by Mrowec et al,[6] in the binary Fe-Cr alloy system. At lower sulfur potentials (1.8 Nm^{-2} and below) the outer layer was found to be $(Fe,Ni)_9S_8$. The intermediate layer was found to be a mixed spinel phase, $Fe(Fe_{2-x}Cr_xS_4)$ similar to that observed in the inner layer of Fe-Cr alloy system.[6]. The innermost layer, which contained either a spinel or chromium sulfide in an

alloy matrix, is similar to that observed by Podhorodeski et al.[10] in the sulfidation of a Ni-Cr alloy having 23% chromium at high temperatures (>700°C) but not at lower temperatures.[10,11]

Comparison with the Stability Field Diagram

The formation of sulfide phases in some cases can be explained with the help of stability field diagrams based on the existence of a local equilibrium. Local equilibrium conditions can only be applied when the chemical potential of the reacting gas mixture and the thermodynamic activity of reacting elements can be defined, as will be the case at the gas-scale interface. Using an appropriate set of conditions for estimating the activities of the various elements present in SAE 310 stainless steel, Gordon and Worrell[12] have constructed the stability field diagrams for the sulfides of Ni, Cr, and Fe. Based on their calculations, NiS will be stable at sulfur potentials greater than 9×10^{2} Nm^{-2}, and FeS will be stable at sulfur potentials greater than 5×10^{-4} Nm^{-2}. These results are consistent with the observations of the present study where at high sulfur potentials (>14 Nm^{-2}) the FeS phase is observed to contain Ni in solid solution. At intermediate sulfur potentials (>10^{-3} Nm^{-2}) where the compound $(Fe,Ni)_9S_8$ was observed in the present study, the compound Ni_3S_2 was calculated to be stable. At very low sulfur potentials (<10^{-3} Nm^{-2}), neither FeS nor $(Fe,Ni)_9S_8$ was observed. Considering the uncertainties associated with thermodynamic data for sulfides, the agreement between the stability field diagram as calculated by Gordon and Worrell[12] and the experimental observations of the present study are considered satisfactory.

Mechanism of Scale Growth

The growth pattern of sulfide layers (Fig. 13) and the results of marker experiments (Fig. 14) suggest that the diffusion of metal ions towards the outer gas-scale interface controls the growth of the outer two layers, whereas the inner layer growth is facilitated by a dissociative mechanism, similar to that originally proposed by Dravnieks and McDonald[13] and by Meussner and Birchenall.[14] Influence of sample geometry on the dissociative mechanism was discussed by Mrowec.[15,16] Mrowec and his associates have shown that the inner layer growth is possible without the participation of inward diffusion of oxidant. The inner layer growth may, however, be further accelerated by the inward diffusion of oxidant through the micro-fissures formed due to lack of plastic deformation, particularly at the corners of the sample. Our marker experiments support this mechanism. If the fissures formed at the boundary of the inner and intermediate layers were above the markers, the growth of the scale in both directions was affected; if the fissures were below the markers, the normal scale growth pattern was observed (Fig. 14). This indicates that the inward diffusion of sulfur through microfissures is negligible and only the dissociation of the primary product at the interface of these two layers is the rate controlling step. This could be concluded from the fact that the hindrance caused by the inert marker would direct the flow of dissociated sulfur vapor to the side affecting the formation of the inner layer below this marker. Lack of formation of the inner layer would also influence the diffusion of metal ions, thus affecting the growth of the outer layer in the vicinity of the marker.

Scale growth mainly manifested by the transport of matter through point defects, such as the one described above, would normally follow a parabolic rate. However, the product scale should be compact and pore-free and there should be no time dependent tortuosity in the reaction mechanism that could either influence the defect-nature of the product lattice or affect the relative rate of diffusing species in a competing reaction due to unsteady state conditions and compositional variations. These conditions are not often met in complex alloy systems where competing reactions between more than one diffusing species occur.

Out of these non-idealities, the following observations were made in the present case. First, the scales appeared to be porous. However, part of the porous appearance of the scales is definitely due to artifacts developed while polishing the samples for optical microscope examination. This could be due to hardness and crystal structure. The shape of artifacts developed during polishing (Fig. 15) could be related to the shape and size of the crystallites observed by scanning electron microscope (Fig. 9). Second, the sulfide present in the form of a dispersed phase constituting the inner layer considerably reduces the cross-sectional area for the outward diffusion. The larger the dispersed area, the smaller will be the area for diffusion; hence, the slower will be the corrosion rate. Third, the composition of the middle layer as well as the inner layer changed until the outer layer started precipitating; this indicated the unsteady state conditions for a considerable length of time. These conditions would influence the reaction rates. The first two conditions would tend to retard the rate of growth; the third would increase the reaction rate as the activity of iron sulfide in the spinel phase increases with time, thus favoring an increase in the rate of diffusion of iron.

During the present study of the sulfidation of 310 stainless steel, neglecting the very initial transient period, two separate regions with a parabolic rate of growth were observed. The parabolic I must be associated with the formation of initial products. These are the formation of mixed spinel layer contiguous to the alloy surface followed by the formation of the dispersed sulfide phase in the metal matrix as described above. Since the end of parabolic I is marked by the end of inner layer growth and a period where the composition of the spinel layer gradually changed, it could be due to unsteady state conditions. Moreover, the reaction carried out at sulfur potentials of 40 Nm^{-2} and above gave only one parabolic relationship. In this case the inner layer is a continuous layer instead of a dispersed phase. This further confirms that the parabolic I is somehow related to the formation of a heterophase inner layer.

During the sulfidation of 310 stainless steel, the slope of the plots of $(\Delta W/A)^2$ versus time increased, indicating that the value of the rate constant $K_{p(II)}$ is greater than that of $K_{p(I)}$. This suggests that the effects caused by the porosity and the reduction in diffusion path due to dispersed phase are negligible. One possible explanation for an increase in the rate constant from parabolic I to parabolic II may be the mechanism and consequences of a formation of inner layer. Initial formation of mixed spinel reduces the sulfur potential at the scale-alloy interface and is dictated by the dissociation pressure of mixed spinel. The dissociation pressure will also be the function of the activity of FeS in the mixed spinel and consequently be a function of the sulfur pressure at which the reaction is carried out. Sulfur produced by dissociation of the spinel would react primarily with chromium causing the depletion of chromium and enrichment of iron and nickel. Since the iron and nickel sulfides are not stable at these low sulfur potentials, the growth of the inner layer would be limited

by the activity of chromium to a certain distance in the alloy where sulfur could penetrate or chromium could diffuse. Considerable increase in the activity of iron and nickel would eventually convert the initially-formed chromium sulfide phase to a spinel phase in the inner layer, and the inner layer growth would cease. As the growth of the inner layer ceases, the concentration of iron and nickel in the spinel phase is increased to the solubility limit of FeS in the $FeCr_2S_4$. This is followed by a relative increase in the diffusion of iron. Once the solubility limit of FeS in the spinel phase is reached, the composition of the spinel phase remains constant and the outer layer starts growing (second parabolic region). Parabolic II was observed over the entire pressure range, from 1.8 Nm^{-2} to 1.5×10^{-2} Nm^{-2}, yet the layers of scale changed from three to two. It is tentatively proposed that the parabolic II is related to the diffusion of metal ions through the spinel phase.

Both the parabolic rate constants yield similar variations with respect to sulfur pressure. This suggests that the diffusing species over the entire range of sulfidation may be identical. In order to interpret the dependence of the parabolic rate constant on sulfur pressure, the diffusion mechanism through the spinel lattice must be understood. No acceptable model has thus far been proposed and it is not even known whether the spinel lattice conforms to the same rules in influencing the ionic lattice defects as do the cubic oxides and sulfides. Schmalzried and Wagner[17] discussed the lattice defect mechanisms in oxide spinels. They point out that, because of the dependence of the activities on oxygen partial pressure, the lattice defects in the spinel must also be a function of oxygen partial pressure. Schmalzried[18] confirmed the increase in the diffusion coefficient with the increasing partial pressure of oxygen in Fe_3O_4. While some guiding principles for the spinels that exhibit a narrow homogeneity range are known, there is no theoretical treatment yet available for the formation of spinels with a wide homogeneity range.[19] Schmalzried,[19] however, showed that the formation of mixed spinel with a wide homogeneity range may follow a parabolic rate of growth. In the present study, the mixed spinel has a wide homogeneity range, where product-phase $FeCr_2S_4$ has extended solubility for FeS. The amount of FeS in the mixed spinel decreased with decreasing partial pressure of sulfur. This could influence the reaction rate and yield a functional dependence of the parabolic rate constant as described by Schmalzried and Wagner.[17] Since the activity of FeS in the mixed spinel phase changes as a function of sulfur pressure, the diffusion rate of Fe in the spinel will change as function of sulfur pressure. Our experimental results gave the functional relationship of approximately $P_{S_2}^{1/4}$. Not knowing the degree of ionization of cation vacancies, this value cannot be given much emphasis. This value is, however, in the range of what one would expect for the diffusion of doubly charged cation vacancies through a P-type, metal-deficit, semiconductor.[20]

Nickel may also play an important role in the sulfidation reaction. The concentration of nickel in the spinel layer was observed to decrease as the sulfur pressure decreased. A maximum drop in the concentration of nickel in the spinel layer was observed to occur at a sulfur potential of 1.5×10^{-4} Nm^{-2}, where the rate of reaction decreased considerably. The solubility of nickel in the spinel phase at this pressure was found to be 0.55%. It is known that FeS as well as Cr_2S_3 are metal deficit P-type conductors.[21,25] The presence of nickel in the crystalline lattice of chromium sulfide results in a decrease in the concentration of cation vacancies

$$2NiS + V''' \rightleftharpoons 3Ni'_{Cr} + 3S \quad (3)$$

Nickel in the crystalline lattice of iron should not cause significant changes. Because it is a mixed spinel, the possibility of substitution of this kind is questionable. The ionic radius of Ni^{2+} is more favorable than Fe^{2+} in the substitution for Cr^{3+}. It is reasonable that nickel in the spinel lattice will reduce the chromium ion vacancies favoring the transport of iron. Alternatively, this could be viewed as a result of the concentration of chromium sulfide in the spinel phase. An increase in the activity of chromium sulfide in the spinel phase would decrease the diffusion rate of iron.

ACKNOWLEDGEMENTS

The authors thank Mr. James Stein and Mr. John Maasberg for their assistance during the experimental work. The constant encouragement from Mr. Dell P. Williams of NASA-Ames Research Center and Mr. Allan V. Levy of Lawrence Berkeley Laboratory is highly appreciated. Mr. Bruce A. Gordon is thanked for providing us with some of his results on stability field diagrams. Financial support from the Materials Science Branch of Ames Research Center, NASA, and the Physical Sciences Division, ERDA, is gratefully acknowledged.

REFERENCES

1. A. J. McNab, "The Materials/Design Interface in Coal Conversion Technology," in Materials Problems and Research Opportunities in Coal Conversion, NSF, OCR Workshop Proceedings, Ohio State University, 16–18 April, 1974.

2. High Temperature Metallic Corrosion of Sulfur and its Compounds, Z. A. Foroulis, Ed., The Electrochemical Society, New York, 1969.

3. K. N. Strafford, Met. Rev., *138*, 153 (1969).

4. "JANAF" Thermochemical Tables, D. R. Stull, Ed., Dow Chemical Co., Midland, Mich., 1967.

5. F. Jellinek, Acta Cryst., *10*, 620 (1957).

6. S. Mrowec, T. Walec, and T. Werber, Oxidation of Metlas, *1*, 93 (1969).

7. T. Narita and K. Nishida, Oxidation of Metals, *6*, 157 (1973); *6*, 181 (1973).

8. S. Zelouf and G. Simkovich, "The Kinetics of Sulfidation of Binary and Ternary Iron Alloys in H_2-H_2S Gas Mixtures," in Ref. 2, pp. 119–131.

9. K. N. Strafford and R. Manifold, Corrosion Sci., *9*, 489 (1969).

10. J. Podhorodeki, J. C. Colson, M. Lambertin, F. Nowack, and J. Kaczor, "Study of the Processes and Kinetics of Corrosion of Nickel-23 w% Chromium and Nickel-20 w% Chromium-1/2 w% Manganese alloys by Sulfur and its Compounds," in Metal-Slag-Gas Reactions and Processes, Z. A. Foroulis and W. W. Smeltzer, Eds. The Electrochemical Society, 1975.

11. G. Romeo, W. W. Smeltzer, and J. S. Kirkaldy, J. Electrochem. Soc., *118*, 740 (1971); La Chimica e l'Industria, *54*, 28 (1972).

12. B. A. Gordon and W. L. Worrell, private communication.

13. A. Dravnieks and H. McDonald, J. Electrochem. Soc., *94*, 139 (1948).

14. R. Maussner and C. Birchenall, Corrosion Sci., *13*, 677 (1957).

15. S. Mrowec, Corrosion Sci., *7*, 563 (1967).

16. S. Mrowec, "Mechanism of High Temperature Metallic Corrosion by Sulfur Vapor," in Ref. 2, pp. 55–109.

17. H. Schmalzried and C. Wagner, Z. Physik, Chem., (NF) *31*, 198 (1962).

18. H. Schmalzried, Z. Physik. Chem., (NF) *31*, 184 (1962).

19. H. Schmalzried, "Chemical Reactions Between Crystalline Solids," in Reactivity of Solids, J. W. Mitchell, R. C. DeVries, R. W. Roberts and P. Cannon, Eds., John Wiley & Sons, Inc., 1969.

20. P. Kofstad, High Temperature Oxidation of Metals, John Wiley & Sons, Inc., New York, 1966.

21. H. Haraldsen, Z. Anorg. Allg. Chem., *246*, 169 (1941).

22. S. Mrowec, Bull. Acad. Pol. Sci., *15*, 517 (1967).

23. S. Mrowec and M. Zastawnik, J. Phys. Chem. Solids, *27*, 1027 (1966).

24. T. Rosenquist, J. Iron Steel Inst., *176*, 37 (1954).

25. D. J. Young, W. W. Smeltzer, and J. S. Kirkaldy, J. Electrochem. Soc., *120*, 1220 (1973).

TABLE 1. CHEMICAL COMPOSITION OF SAE 310

Iron	52.59	Cobalt	0.38
Chromium	24.76	Copper	0.21
Nickel	19.05	Carbon	0.05
Manganese	1.70	Phosphorous	0.035
Silicon	0.72	Sulfur	0.010
Molybdenum	0.49		

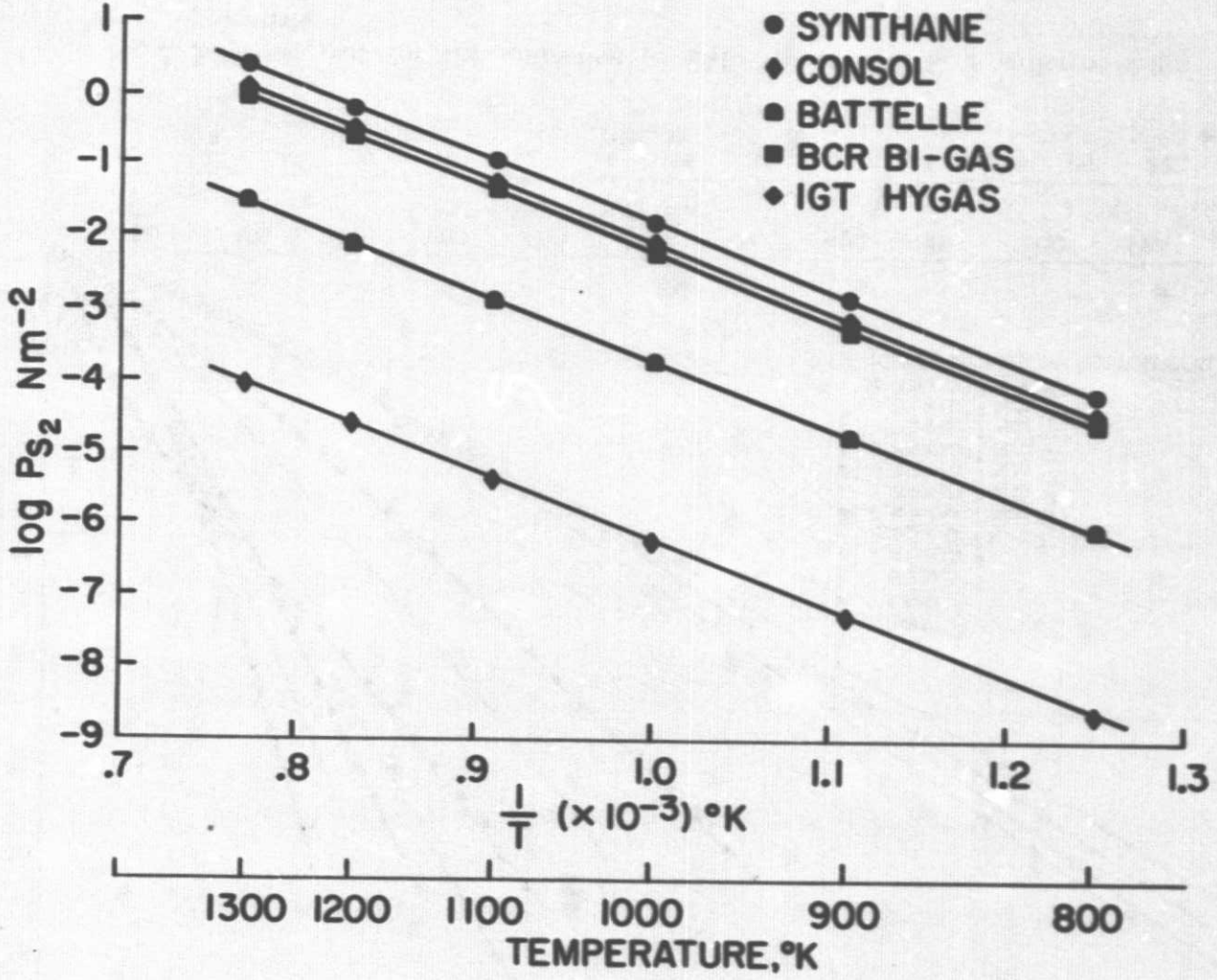

Fig. 1. Sulfur potentials in coal conversion processes as a function of absolute temperature.

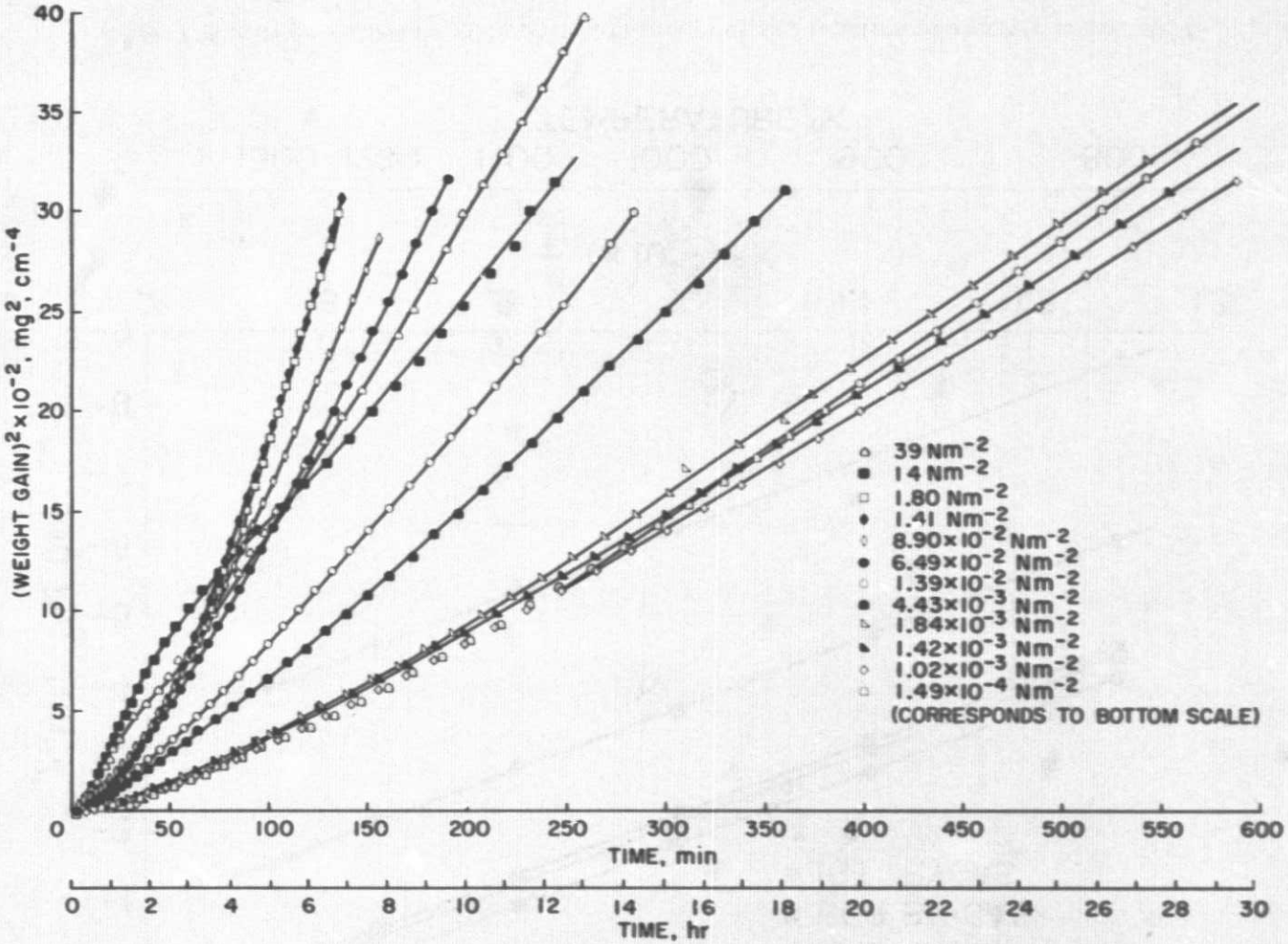

Fig. 2. Parabolic plot for the sulfidation of SAE 310 at 1065 K at different sulfur potentials.

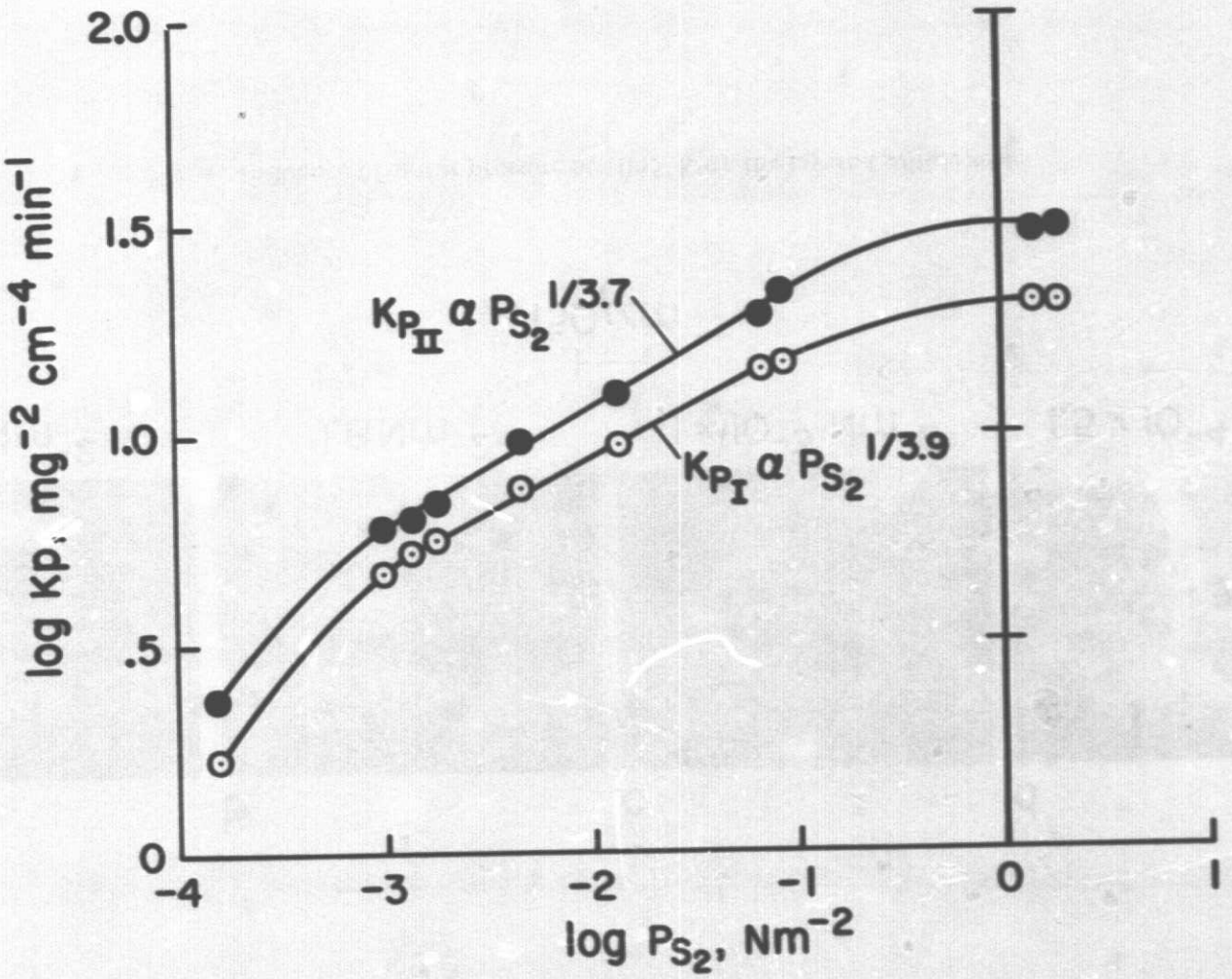

Fig. 3. Influence of sulfur potentials on the parabolic rate constants for the sulfidation of SAE 310 at 1065 K.

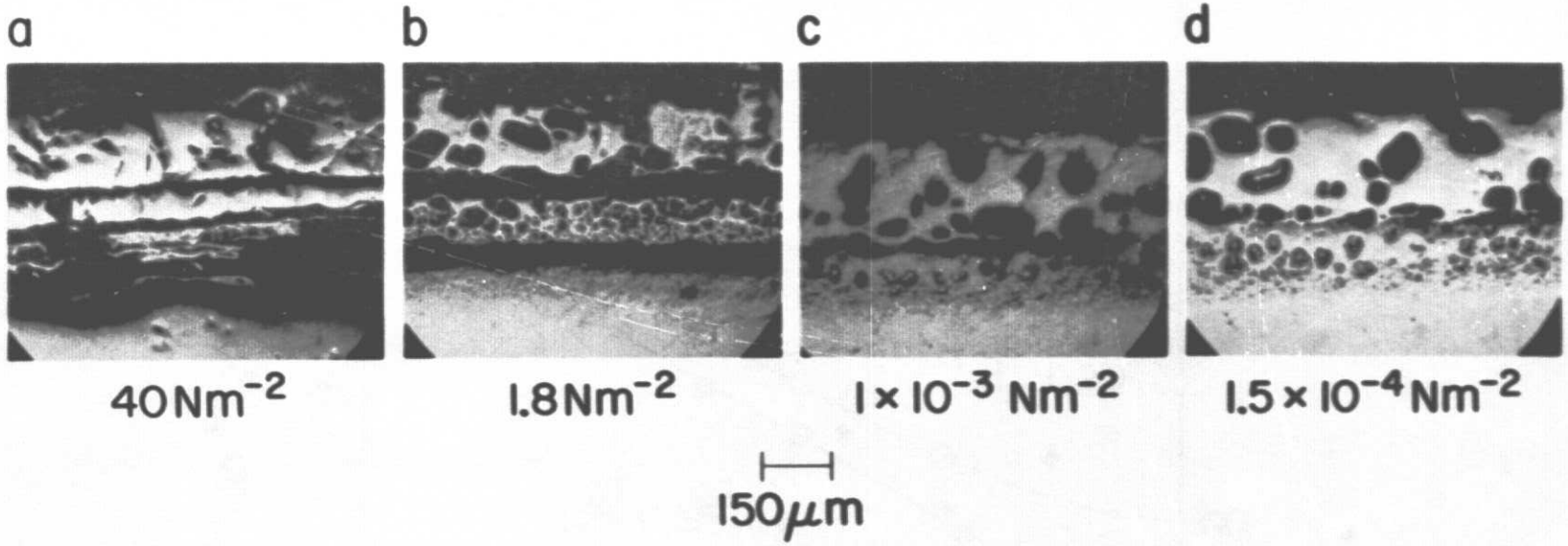

Fig. 4. Influence of sulfur pressure at 1065°K on the layered sulfide scale.

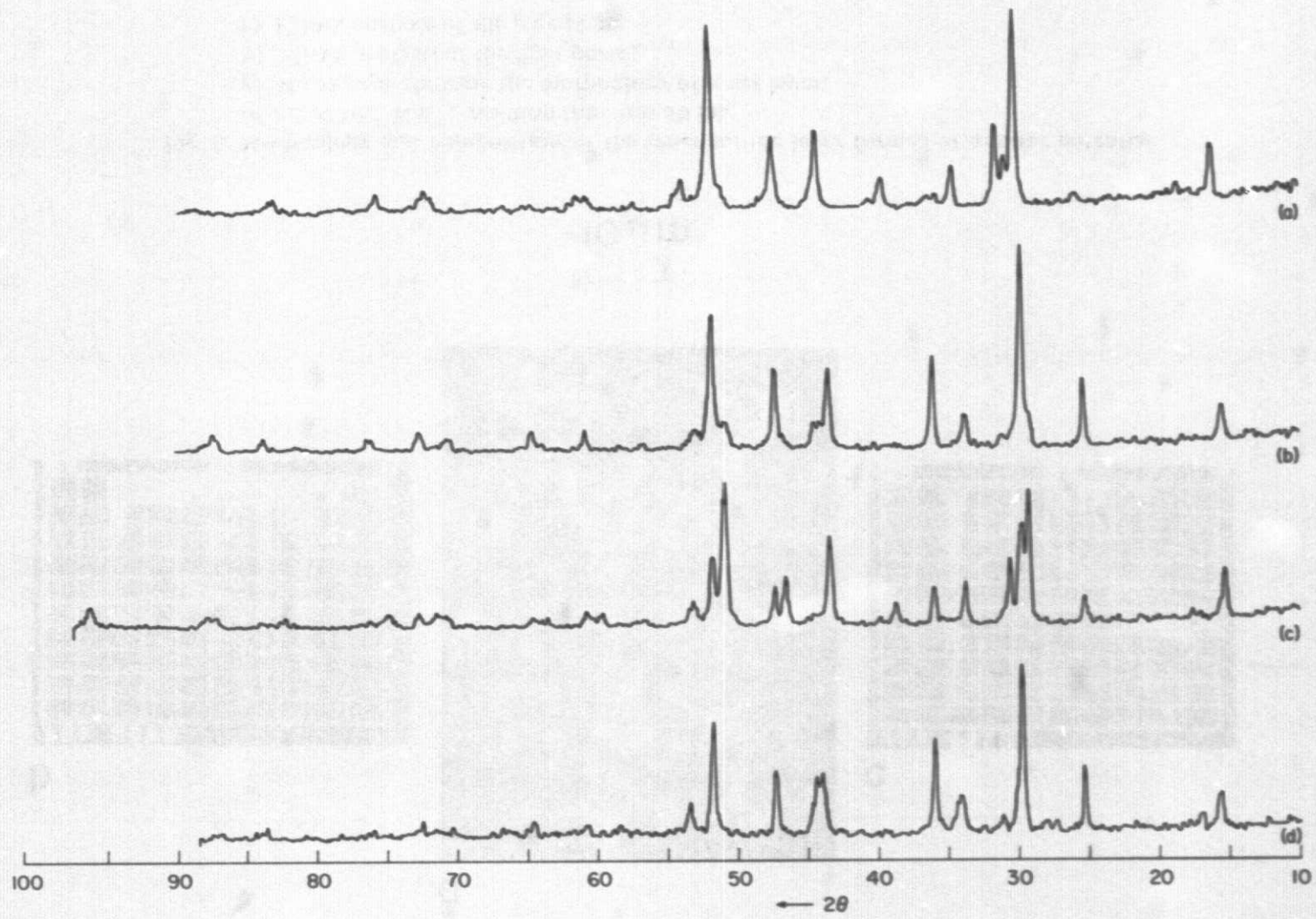

Fig. 5. Diffraction patterns for the layers of the sulfide scale formed at a sulfur potential of 1.8 Nm^{-2}: a) Diffraction pattern for the outer layer; b) Diffraction pattern for the middle layer; c) Diffraction pattern for the mixture of outer and middle layers; d) Diffraction pattern for the inner layer.

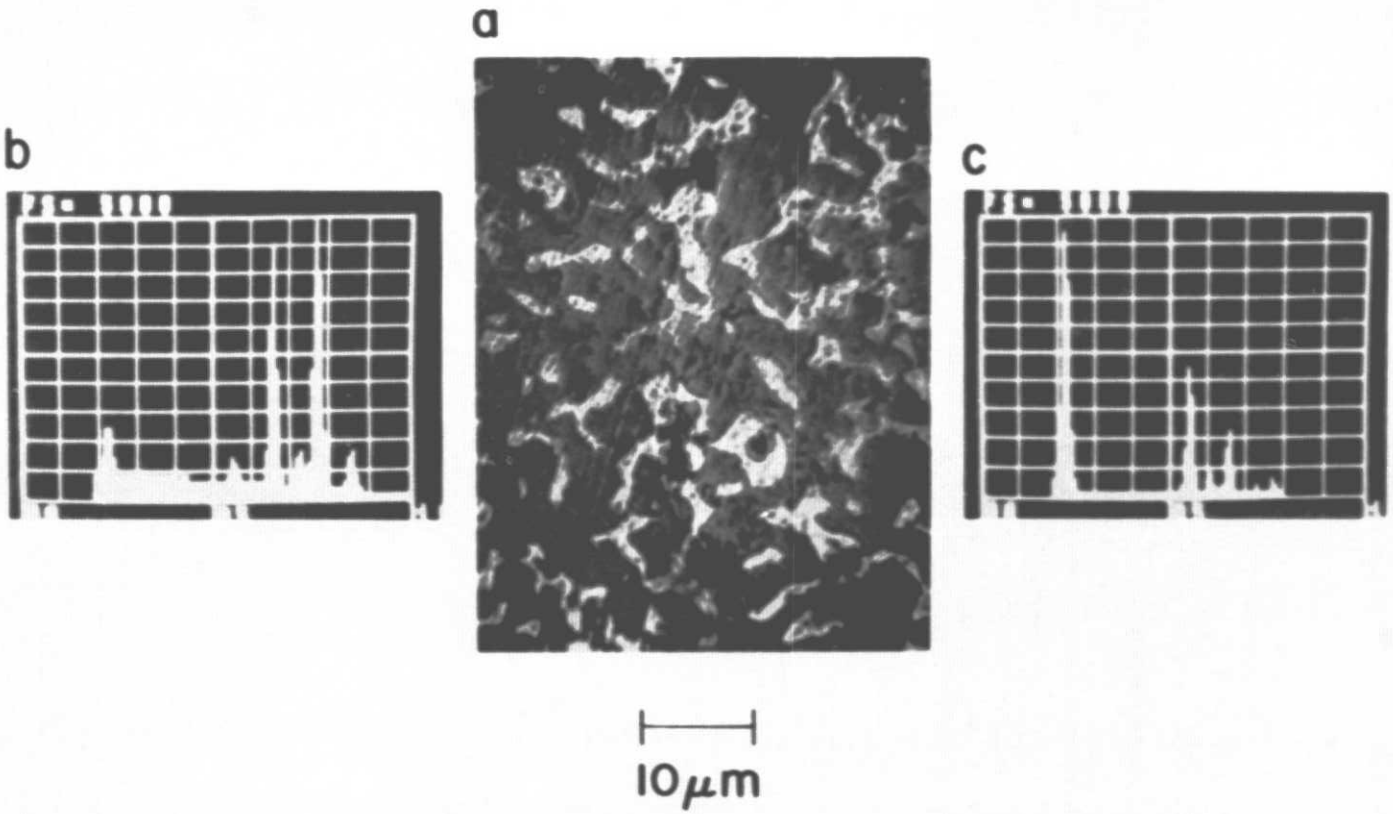

Fig. 6. Morphology and composition of the inner sulfide layer formed at a sulfur potential of 1.5×10^{-4} Nm^{-2}; reaction time was 30 hr:
a) Micrograph showing the morphology of inner layer;
b) EDAX analysis of the light phase;
c) EDAX analysis of the grey phase.

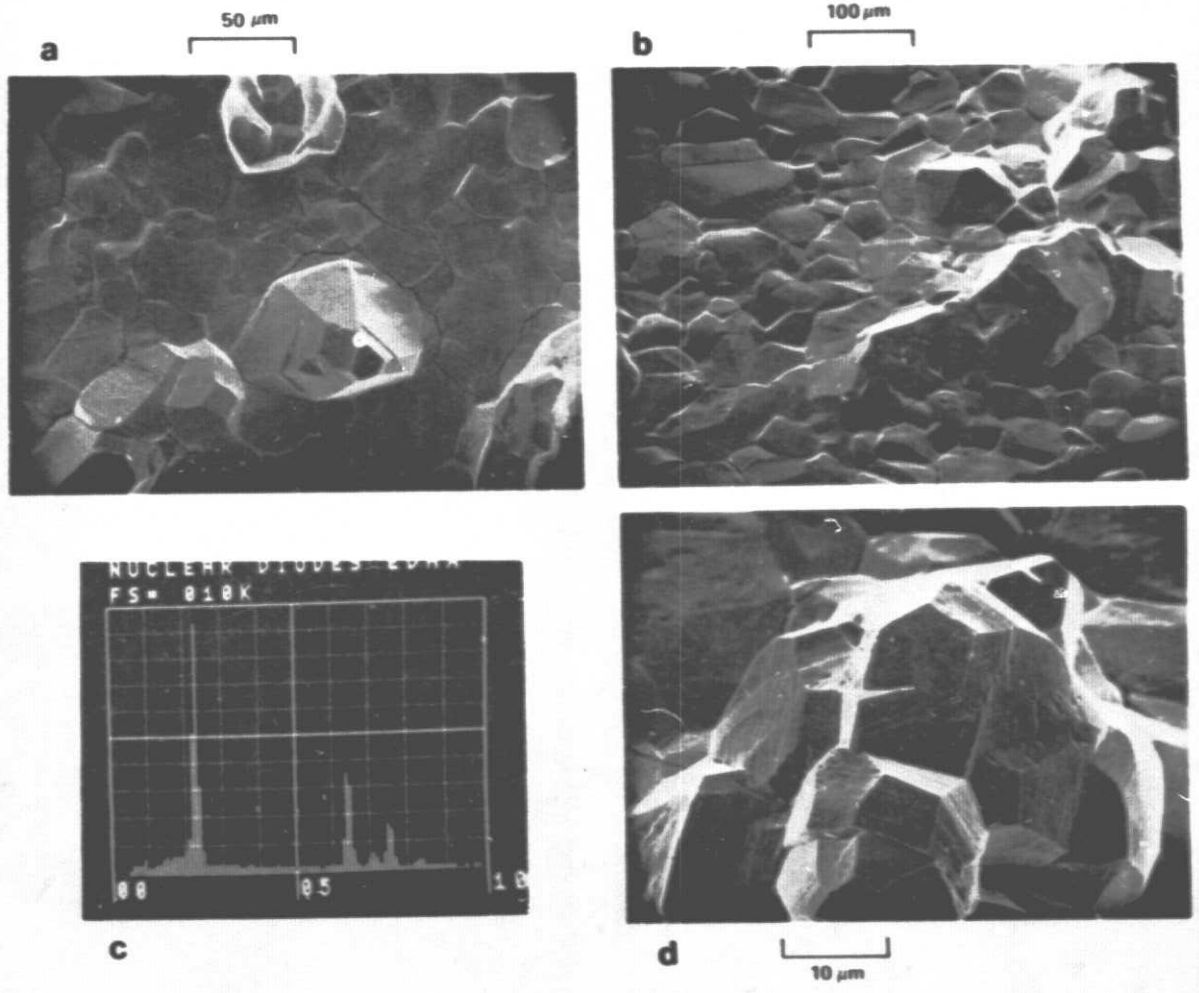

Fig. 7. Microstructure and composition of the top surface of the outer layer (gas-scale interface) formed at a sulfur potential of 9×10^2 Nm^{-2}; t = 5 hr. a), b), and d) show the morphological variations, and c) gives the composition of the columnar crystal at the spot indicated in (a).

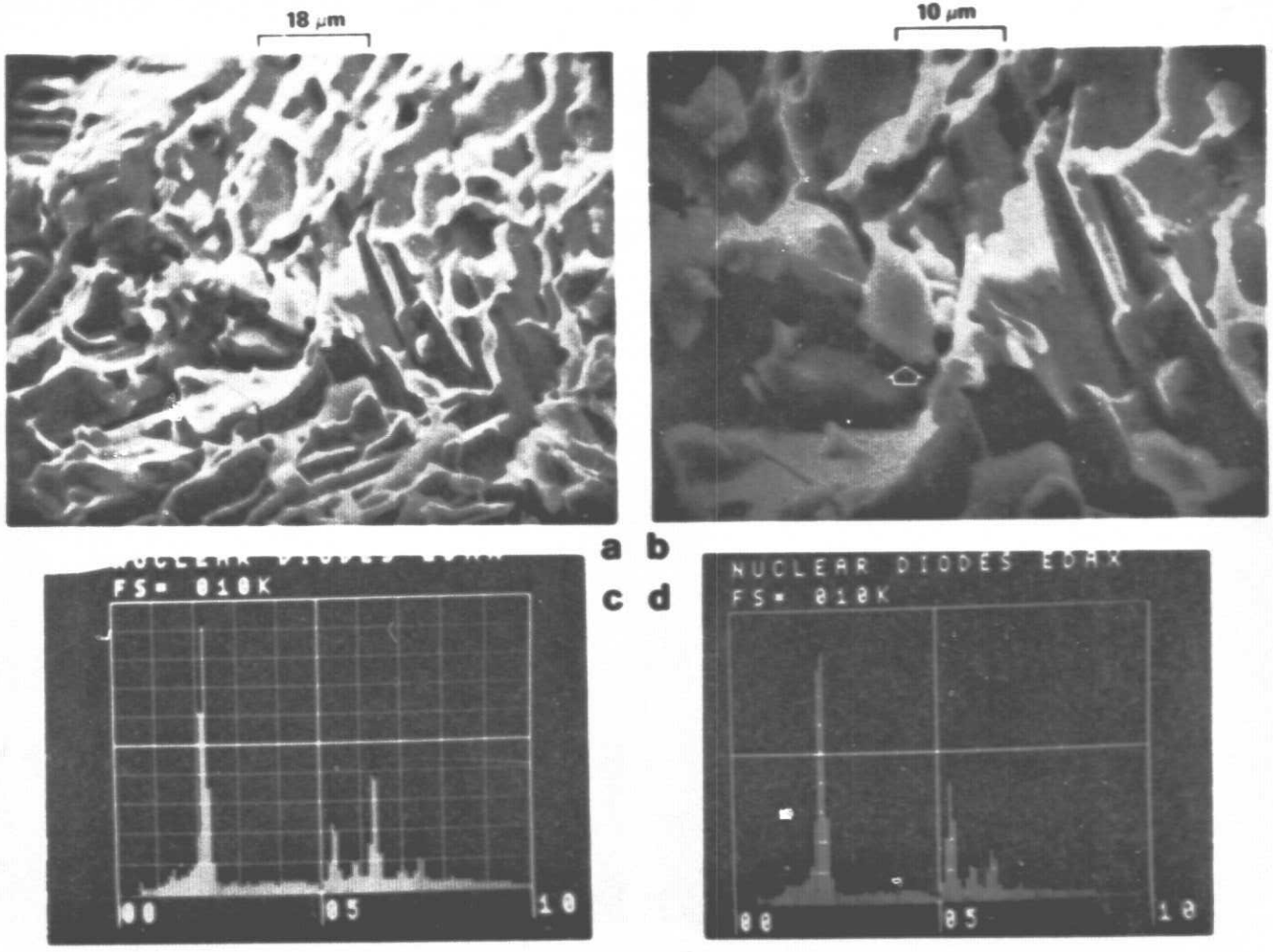

Fig. 8. Microstructure and composition of the bottom side of the outer layer: a) Scanning electron micrograph of the surface; b) Same as in (a) but higher magnification; c) EDAX analysis of the overall surface shown in (a); d) EDAX analysis of grain indicated by arrow in (b).

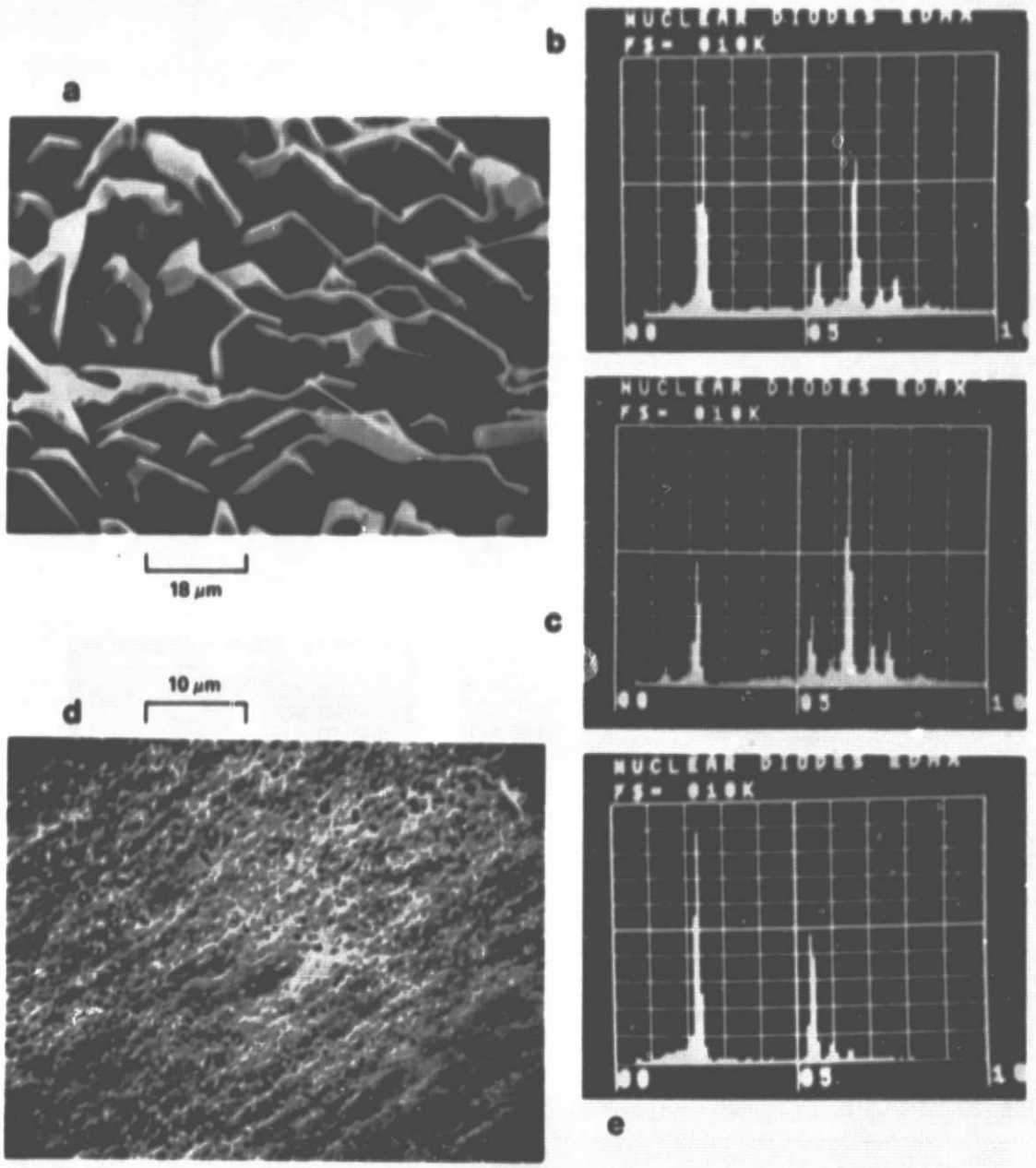

Fig. 9. Microstructure and composition of the top and bottom surfaces of the middle layer formed at $P_S = 9 \times 10^2$ Nm^{-2}:

a) Scanning electron micrograph of the top surface;
b) EDAX analysis of overall area shown in (a);
c) EDAX analysis of crystallite indicated by arrow in (a);
d) Scanning electron micrograph of the bottom surface;
e) EDAX analysis of the overall area shown in (d).

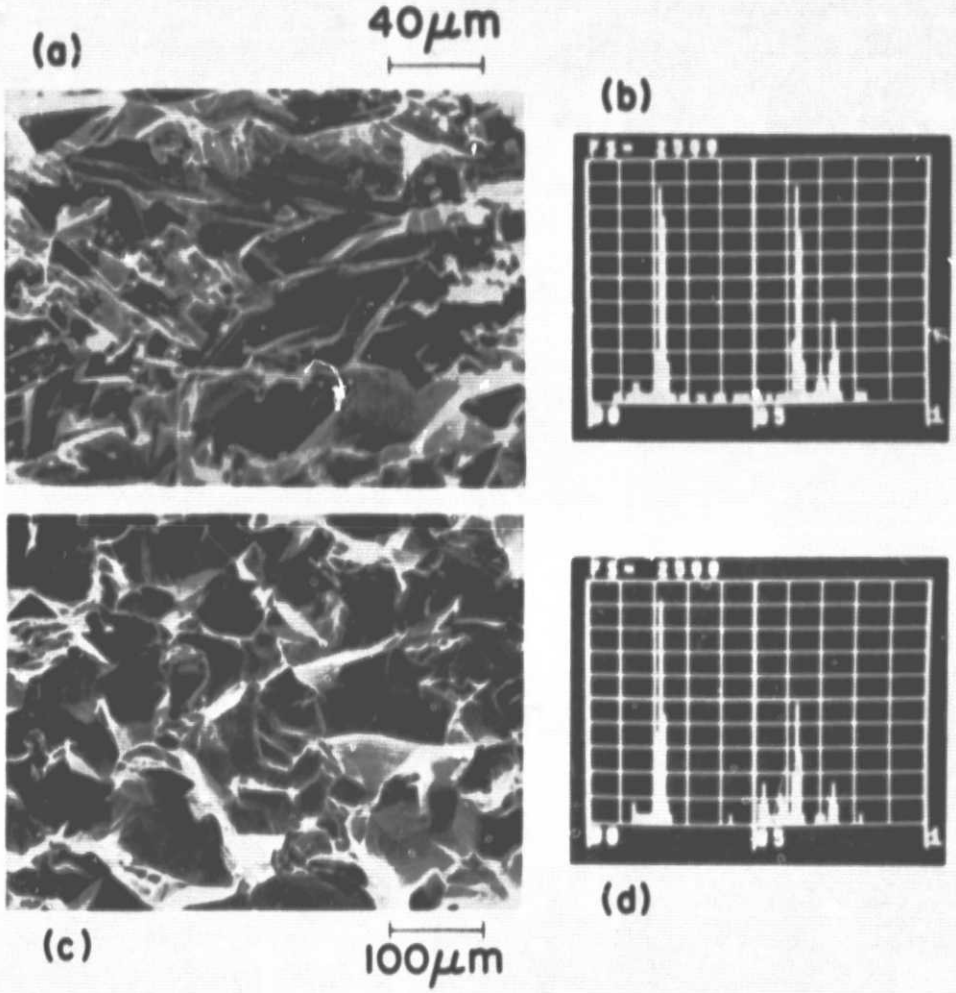

Fig. 10. Microstructure and composition of the top surface of the upper layer, a) and b); top surface of the middle layer, c); and d) formed at 1.5 Nm^{-2}.

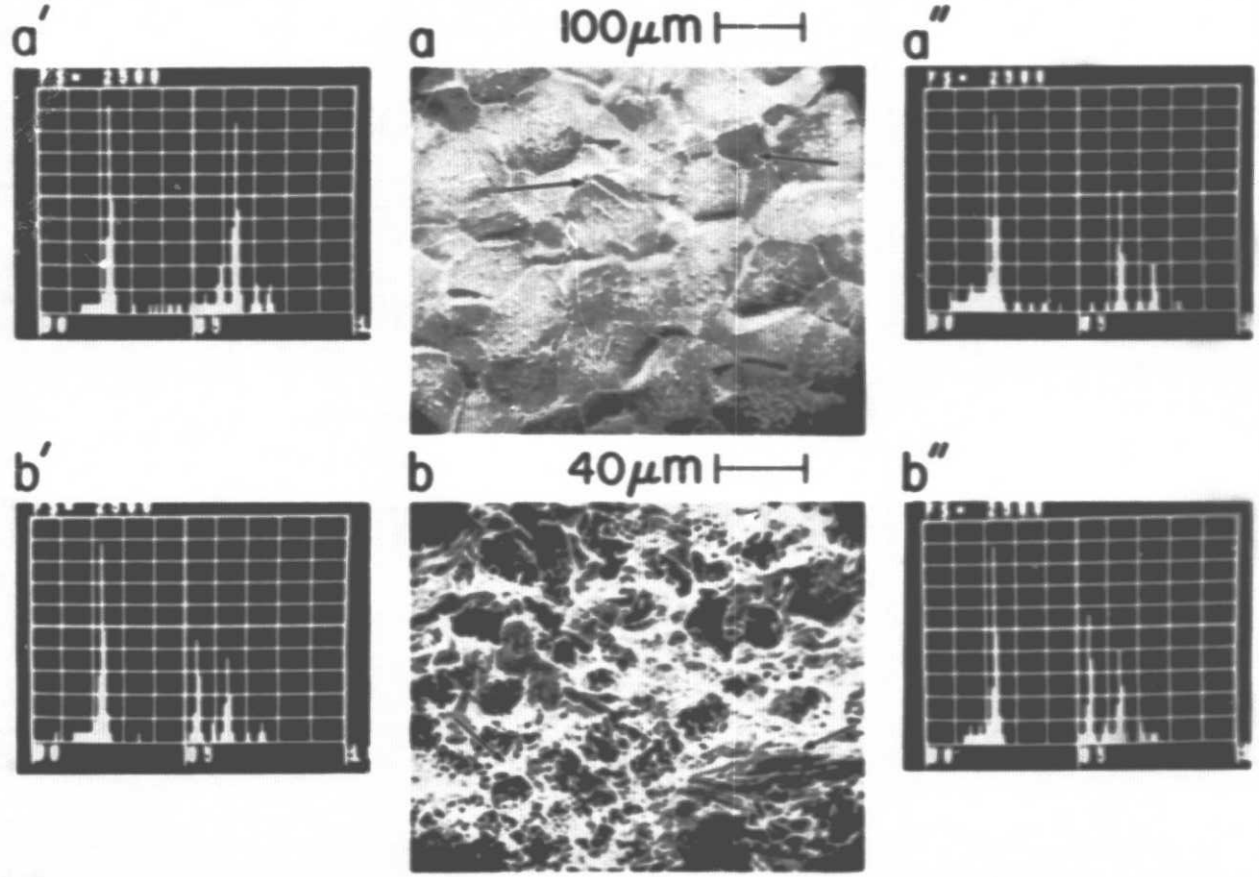

Fig. 11. Microstructure and composition of the sulfide layers formed at a sulfur potential of 1×10^{-3} Nm^{-2}; t = 10 hr: a) SEM of the top surface of outer layer; a') EDAX analysis of small crystallites indicated by arrow; a") EDAX analysis of crystal surface indicated by arrow; b) SEM of the bottom surface of the top layer; b') EDAX analysis of crystallites indicated by arrow; b") EDAX analysis of the jagged area indicated by arrow.

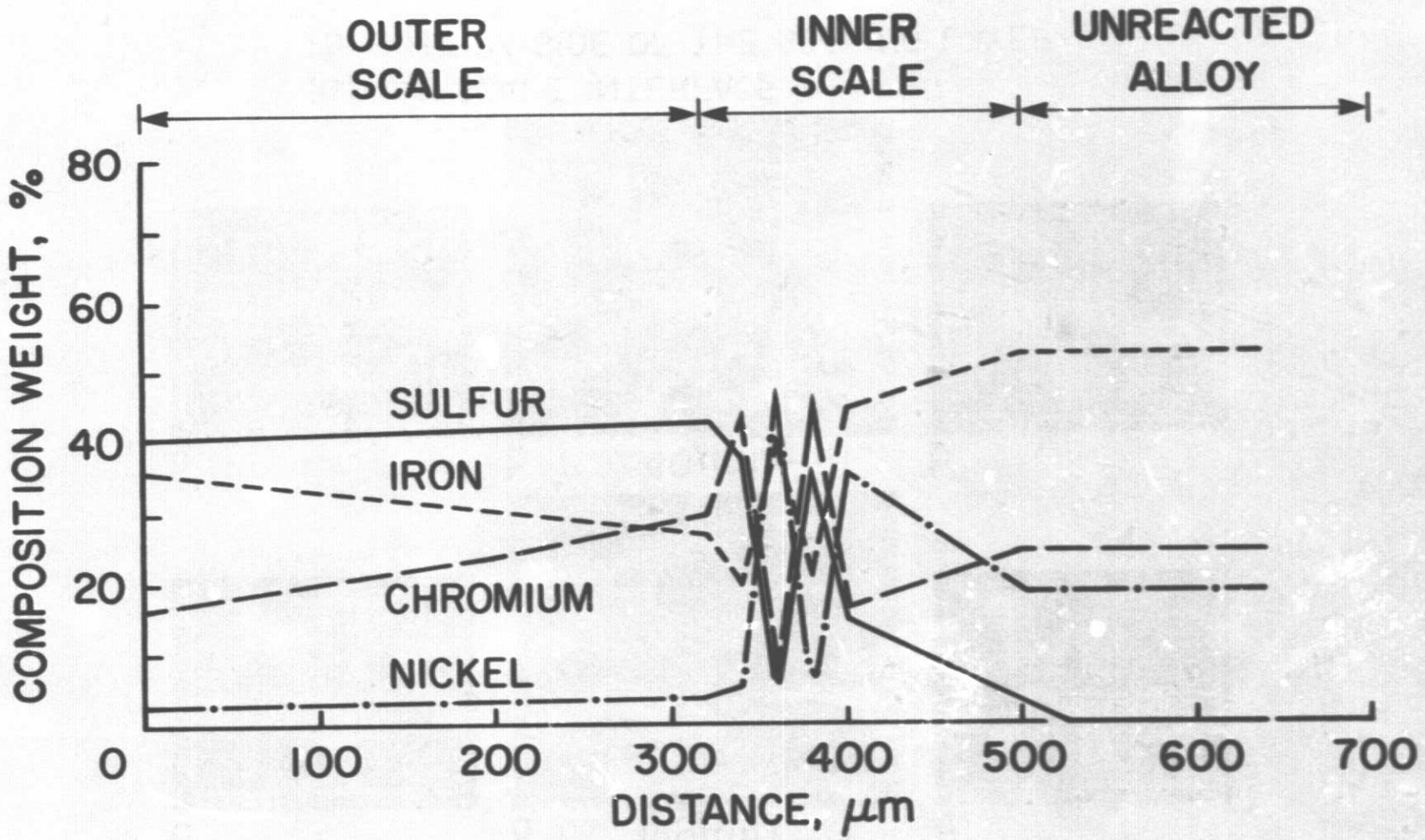

Fig. 12. Distribution profile after sulfidation for 10 hr at a sulfur potential of 1×10^{-3} Nm^{-2} as analyzed by electron microprobe.

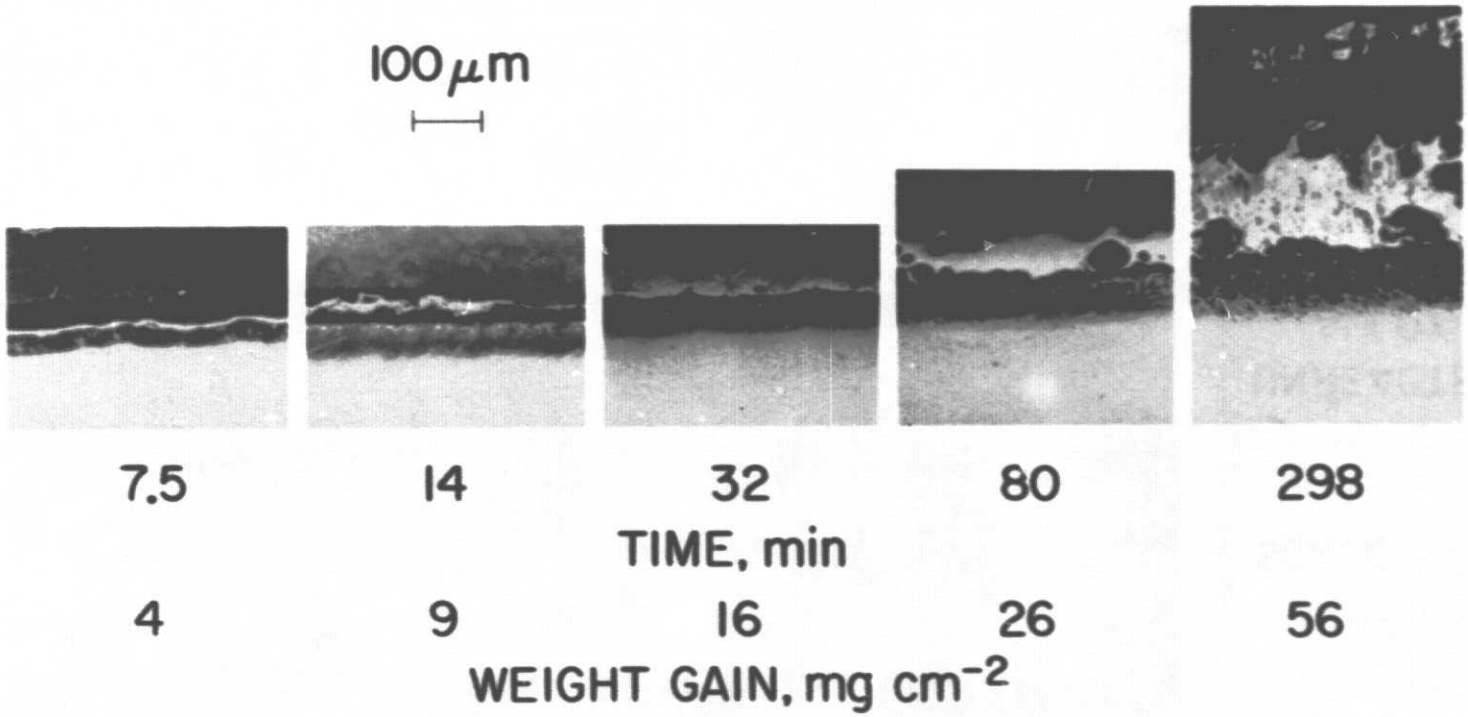

Fig. 13. Sulfide scale thickness as a function of reaction time at a sulfur potential of 1.4×10^{-2} Nm^{-2}.

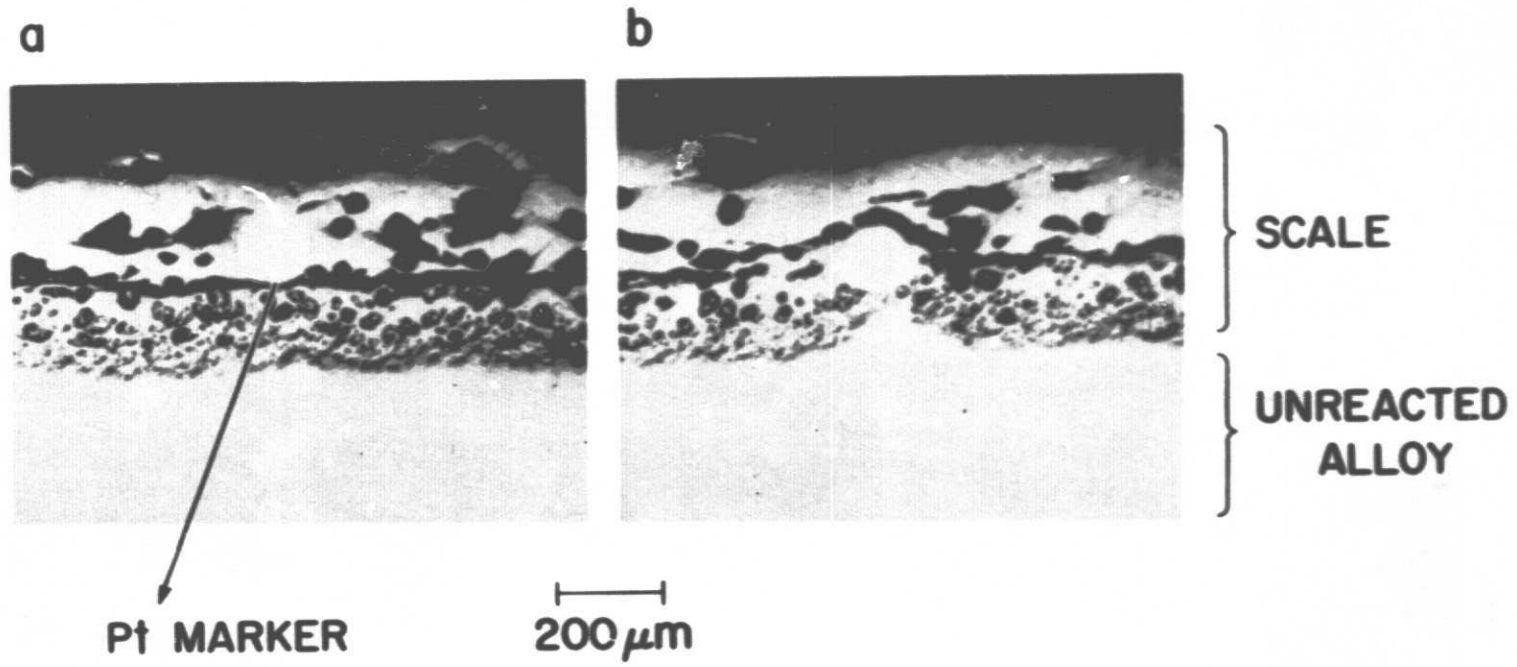

Fig. 14. Transverse section of the sulfide scale showing the position of inert markers. The sample was reacted for 30 hr at a sulfur potential of 1.5×10^{-4} Nm^{-2}.
a) Micrograph showing the fissure below the marker;
b) Micrograph showing the fissure above the marker.

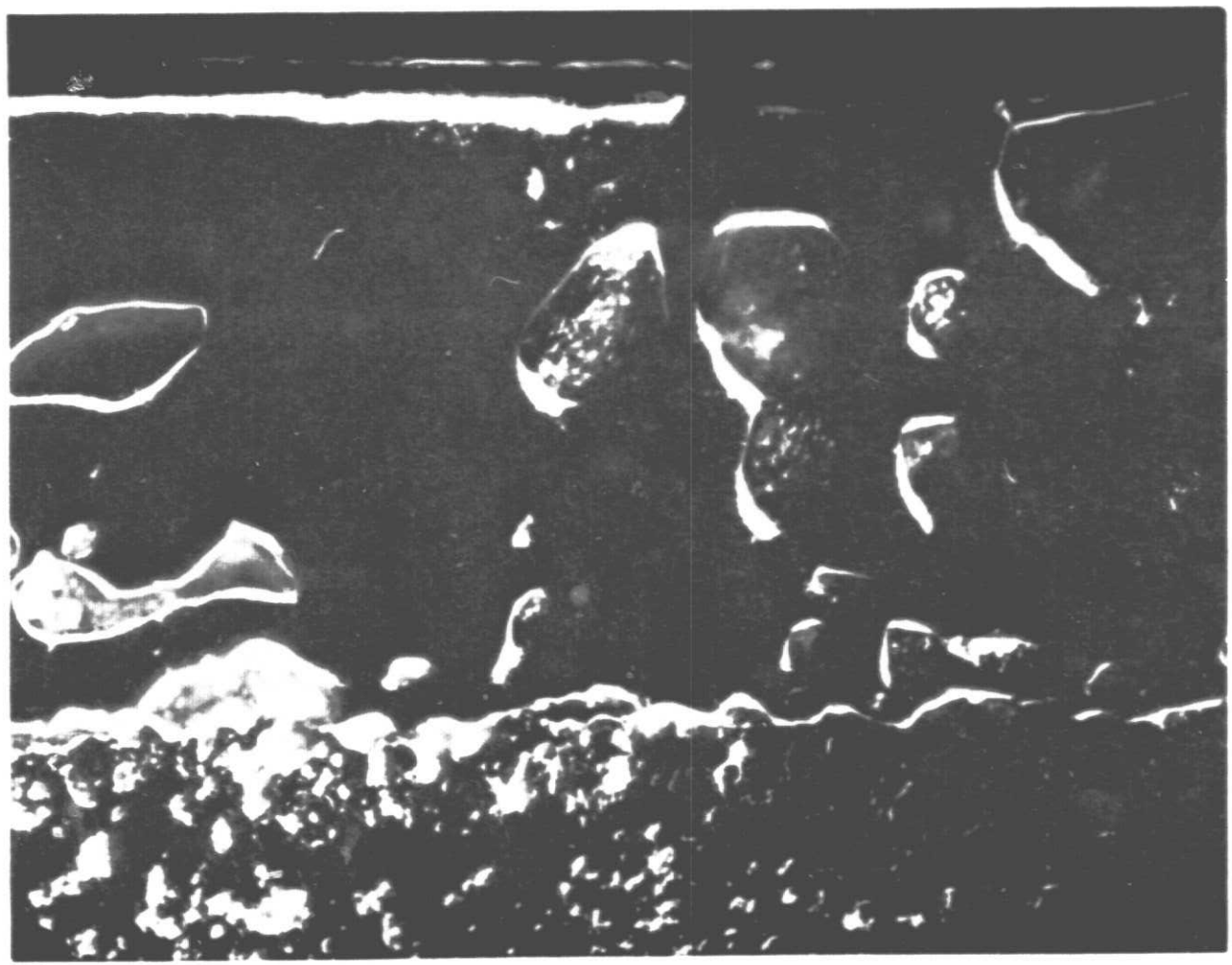

Fig. 15 Micrograph showing the shape of artifacts developed during polishing.